ACS APPLIED POLYMER MATERIALS

pubs.acs.org/acsapm
Article

Flexible Thin-Layer Strain Sensors Made of Natural Rubber

Sutthinee Keawmaungkom, Panithi Wiroonpochit,* Sasitorn Srisawadi,* Siwaporn Srimongkol, Jirasak Wong-Ekkabut, Saree Phongphanphanee, Sarun Phibanchon, Yusuf Chisti, and Nanthiya Hansupalak*

Cite This: ACS Appl. Polym. Mater. 2025, 7, 12468−12479
Read Online

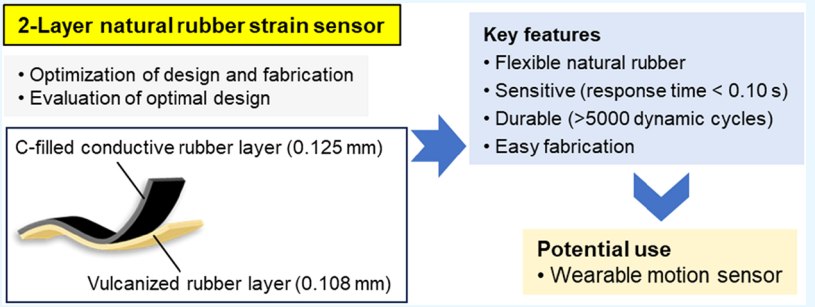

ABSTRACT: High-performance 2-layer polymeric strain sensors based on natural rubber (NR) and the electrically conductive filler acetylene black (AB) were fabricated. The structure of the sensors and the thickness of the polymer layers were optimized. An optimal sensor design comprised a 2-layered configuration with a nonconductive rubber layer (0.108 mm thick) bound to an AB-containing conductive rubber layer (0.125 mm thick). This configuration had superior mechanical properties with a gauge factor (*GF*) peaking at 10,607 during the initial stretching cycle and stabilizing at approximately 2800 from the second cycle onward, within a strain range of 54−71%. The sensor maintained high linearity (correlation coefficient = 0.99). It demonstrated outstanding long-term durability, retaining functionality over 5000 dynamic stretching cycles in the 10−50% strain range. Within this strain range, the sensor had a rapid response time of 0.06−0.10 s. A simple fabrication process, combined with high sensitivity, rapid response, and excellent durability underscored its potential for use in human motion detection and other wearable applications.

KEYWORDS: *natural rubber strain sensor, flexible strain sensor, layered polymer strain sensor, conductive rubber composites, wearable strain sensor*

1. INTRODUCTION

Flexible resistive strain sensors made of conductive polymer composites are critical components in wearable technologies, finding widespread use in textile engineering and medical devices.[1−3] A strain applied to the sensor changes the electrical resistance of the conductive network embedded in the sensor, allowing the strain to be measured.[4−6] The traditional sensor designs often suffer from unsatisfactory mechanical properties and poor sensing characteristics because of the high loadings of the conductive filler typically necessary for sufficient conductivity.[6] Alternative multilayer composite designs such as the bilayer and the sandwich configurations have been developed for enhancing the physical and sensory characteristics.[6−9] The multilayer designs allow the conductive layer to be separated from the strength-providing layer so that the sensor combines good sensory performance and adequate mechanical properties. Flexible sensors based on thin multilayer polymer composites are sensitive, broadly applicable, relatively inexpensive, lightweight, and easy to fabricate.[6−9] The polymers used in making resistive strain sensors include polydimethylsiloxane,[10] polyurethane,[11] elastomeric silicone rubber,[12] the biodegradable polybutylene adipate-*co*-terephthalate (Ecoflex),[13] and natural rubber.[14] The conductive fillers are typically carbon-based materials (e.g.: carbon nanotubes;[15] graphene;[16,17] carbon black[18]), MXenes,[19] metal particles,[10] and metal ions.[20]

Natural rubber (NR) is especially suitable as a strain sensor matrix because of its high elasticity, excellent fatigue resistance,[14] and inherent flexibility for seamless integration into wearable systems.[21] Harvested sustainably from the rubber tree (*Hevea brasiliensis*), NR is biodegradable and an attractive alternative to petroleum-derived synthetic materials such as the often-used poly(dimethylsiloxane) (PDMS) and thermoplastic

Received: June 25, 2025
Revised: September 2, 2025
Accepted: September 8, 2025
Published: September 16, 2025

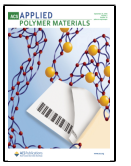

polyurethane (TPU). While pristine NR is mechanically weak, its properties and durability are easily enhanced by various prevulcanization processes which cross-link the rubber molecules into a network of covalently bound chains. Among prevulcanization process, the sulfur-based method is particularly effective. Sulfur-prevulcanized natural rubber (PVNR) manifests enhanced elasticity, fatigue durability, and shape recoverability compared to native NR. These attributes are important for producing robust and stable strain sensors for long-term use. Numerous PVNR-based strain sensors have been reported.[14,21,22] The techniques used for fabricating these sensors include filling, coating, casting, sandwiching, and adsorptive methods. The different fabrication methods result in sensors with markedly different performance characteristics, especially in terms of the gauge factor (*GF*), strain range, response time, and cyclic stability.[21] These methods notwithstanding, no work has been reported on fabrication of PVNR-based strain sensors involving a bilayer polymer composite architecture in which the conductive and the elastic layers are structurally separated. Such a design is promising for mitigating the typical trade-offs between mechanical integrity and electrical sensitivity observed in conventional single-phase sensor systems.[6]

To address the gap identified above, this study focused on the use of acetylene black (AB, high purity nanosized variant of carbon black) as the conductive filler in PVNR matrices. AB has several desirable attributes for sensor applications, including high thermal conductivity, low moisture absorption, a high capacity of absorption of liquids, elasticity, and compressibility.[23,24] Its nanoscale particle size and high specific surface area are particularly good for generating robust conductive networks within elastomeric matrices. There have been no reports on the use of AB in PVNR-based sensors except our own prior work which employed a different filling method.[22] In the cited study,[22] the sensor achieved a *GF* of only 9 over a strain range of 0−10%. Therefore, the current study investigated whether sensory performance could be improved by adopting a bilayer configuration in sensor fabrication. Thus, in the present work, resistive strain sensors comprising sulfur-prevulcanized natural rubber (S-PVNR) and acetylene black as the active composite system were investigated. Both single-layer and bilayer sensor configurations were fabricated, and their performance was evaluated in terms of sensitivity, stretchability, and stability under dynamic loading. While the present study did not involve human testing, the performance characteristics of the developed sensors indicated a strong potential for future integration into wearable electronic systems, particularly in applications that would benefit by adopting sustainable and biodegradable materials.

2. MATERIALS AND METHODS

2.1. Materials. Sulfur-prevulcanized natural rubber (PVNR) latex (dry rubber content (DRC) = 55% w w^{-1}) was prepared by mixing high ammonia concentrated natural rubber (NR) latex (HA latex; Natural Art and Technology Co., Ltd., Thailand) with sulfur and other additives (Table 1) in a mechanically agitated (300 rpm) beaker.[14] This mixture was then heated without mixing on a water bath (50 °C) for 3 h to complete the sulfur prevulcanization process. Acetylene black (AB) AB50 (particle size range of 30−50 nm) was a gift from IRPC Public Co., Ltd., Thailand. Carboxymethyl cellulose (CMC; average particle size of 50 μm; weight-averaged molecular weight = 1.5×10^6 kg $kmol^{-1}$) was purchased from T.C.S Pacific Ltd., Thailand. CMC was used as a dispersant for the carbon nanoparticle dispersions.[25] Sodium dodecyl sulfate (SDS) and all other chemicals (Table 1) were from Lucky Four (Thailand). All aqueous solutions were prepared using deionized (DI) water.

Table 1. PVNR Latex Compound (55% DRC) Formulation

component	amount (phr[a])
HA latex (60% DRC)	100
sulfur (S)	1
zinc diethyldithiocarbamate (ZDEC)	1
zinc 2-mercapto benzothiazole (ZMBT)	1
poly(dicyclopentadiene-cop-cresol) (CPL)	1
zinc oxide (ZnO)	5
potassium hydroxide (KOH)	0.1
deionized water	15

[a]Parts per hundred (by mass) of rubber (phr).

2.2. Preparation of Carbon Composited Conductive Natural Rubber (CNR) Latex. The formulation in Table 2 was used. A 5% SDS solution (5 g SDS in 100 mL deionized water) was heated and maintained at 40 °C. Acetylene black was added with stirring at 300 rpm. After 15 min, the mixing speed was raised to 400 rpm and CMC was added. The mixing continued for a further 15 min. The sulfur-prevulcanized natural rubber (S-PVNR) latex (see Section 2.1) was then added to the mixture and mixing (400 rpm) continued at 40 °C for a further 15 min. Heating was then stopped, but mixing continued for 45 min to obtain the conductive natural rubber (CNR) latex.

Table 2. CNR Latex Compound Formulation

component	amount (phr[a])
S-PVNR latex (55% DRC)	100
sodium dodecyl sulfate (SDS, 5%)	100
acetylene black (AB)	5
carboxymethyl cellulose (CMC)	0.5

[a]Parts per hundred (by mass) of rubber (phr).

2.3. Fabrication of 1-Layer and 2-Layer Strain Sensors. Strain sensors were fabricated using a GN-VC-20H hot film coating machine (Gelon; Shandong, China) with the film applicators of the required gap height (either 0.5 mm, or 1 mm, depending on experiment) to control film thickness. For the 1-layer sensor, CNR latex was coated on a transparent polyester sheet (100 mm × 210 mm) by moving the film applicator across the polyester sheet at a steady speed of 15 mm s^{-1}. The coated sheet was then dried in an oven at 70 °C for 1 h. The sensor preparation process is depicted in Figure 1.

The 2-layer sensor comprised of two parallel polymer layers bound to each other. The first layer (the PVNR layer) was made using the same method as described above for the 1-layer sensor but by using the PVNR latex instead of the CNR latex. The PVNR-coated polyester sheet was dried inside the coating machine by heating to 60 °C for 1 min. Subsequently, the CNR latex was coated on the dried PVNR layer using a film applicator that moved at the speed specified earlier. This formed the CNR layer denoted as the second layer. The entire polyester sheet supporting the two coated layers was dried in an oven at 70 °C for 1 h. The preparation process is outlined in Figure 1. Each dried film comprising either 1-layer or 2-layers was cut into three identical specimens (20 mm × 80 mm) for subsequent testing (Figure 1).[14]

2.4. Characterization. **Film morphologies** of NR/AB strain sensors were characterized by using optical microscopy (Olympus CX31 HD digital microscope; Olympus, Tokyo, Japan), transmission electron microscopy (TEM; 80 kV, HT7800; Hitachi, Tokyo, Japan) and field emission scanning electron microscopy (1 kV, FESEM, JSM-7800 F Prime; JEOL, Tokyo, Japan). The optical images were used for determining the layer thicknesses using the ImageJ software (https://imagej.net/ij/). **Mechanical properties** of the sensors and films were measured according to the Standard ISO 37 in the tension

https://doi.org/10.1021/acsapm.5c02305
ACS Appl. Polym. Mater. 2025, 7, 12468−12479

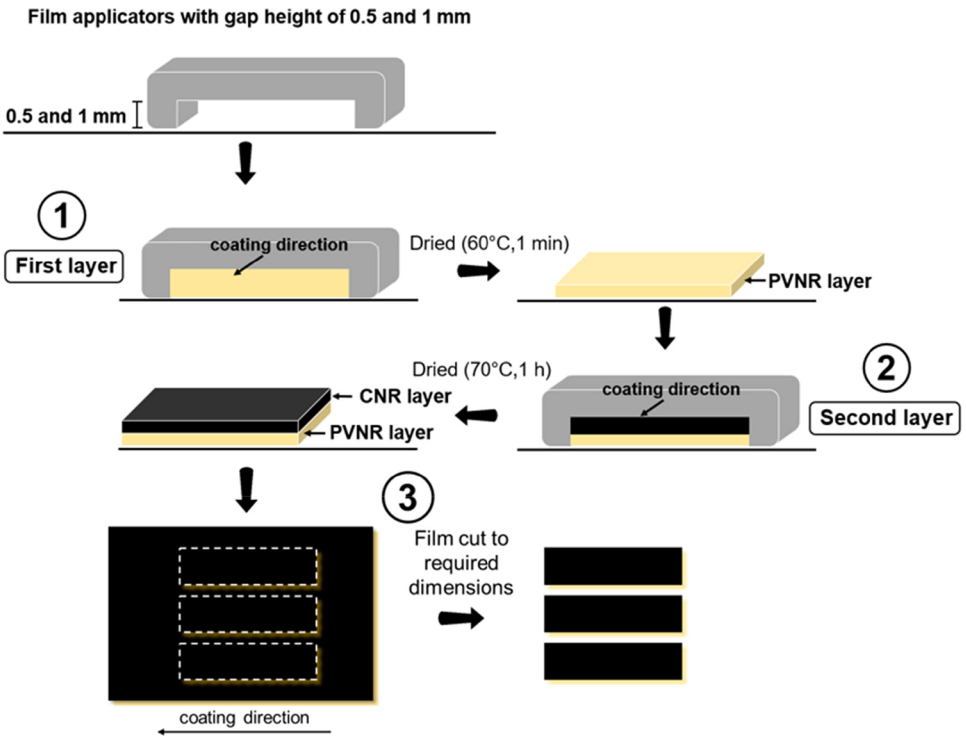

Figure 1. Preparation process for the films. The film applicator with the required gap height is shown at the top. In the first step (circled numbers), the applicator channel was filled with the PVNR latex compound (pale yellow) to form the PVNR layer. Subsequently, in step 2, the applicator was filled with the CNR latex compound (black) and the CNR film was coated on the PVNR film. Step 2 was used only if 2-layer sensors were being made. The water in the latex layers was removed by heating. In step 3, the dry film was cut into three identical pieces measuring 20 mm × 80 mm.

mode using a universal testing machine (NARIN; NRI-TS500−20B (Extra), Thailand) at 25 °C and a 1 kN load cell. The crosshead speed was 500 mm min^{-1}. **Strain sensor performance** was tested using a stretching test bench connected to a high-precision multimeter (HIOKI, DT 4352, Japan). Sensitivity and hysteresis tests were conducted over 100 stretch−release cycles, with the strain varying from 0% to the maximum measurable strain (stretchability) beyond which the resistance (R) exceeded the instrument's range. A data logger (Keithley 34972A, USA) recorded R during each stretching and release cycle. Sensitivity was quantified as the gauge factor (GF, i.e., the ratio of relative change in electrical resistance to the mechanical strain) calculated using the following equation

$$GF = \frac{\Delta R/R_0}{\varepsilon} \quad (1)$$

In the above equation, $\Delta R/R_0$ (%) was the change in relative resistance during stretching ($\Delta R = R - R_0$; R (Ω) = resistance with the applied strain, and R_0 (Ω) = resistance without the applied strain) and ε (%) was the applied strain. The linearity was assessed by using the correlation coefficient value (r^2) of the linear correlation between the relative resistance ($\Delta R/R_0$) and the applied strain (ε).

The change in relative resistance, i.e., $\Delta R/R_0$, during stretching and retraction could differ due to hysteresis, a consequence of softening or deformation of material. The degree of hysteresis (DH, %) was calculated using the following equation

$$DH(\%) = \frac{Y_{\text{unloading}} - Y_{\text{loading}}}{Y_{\text{unloading}}} \times 100 \quad (2)$$

where $Y_{\text{unloading}}$ was the $\Delta R/R_0$ value during retraction (unloading) and Y_{loading} was the $\Delta R/R_0$ value during stretching, or loading. The DH was evaluated at the strain at which the difference between the $\Delta R/R_0$ values for loading and unloading was the largest.

The dynamic cyclic performance of the sensor was tested by subjecting it to 5000 stretch−release cycles with constant strain and recovery rates of 30 mm s^{-1}. During this test, the resistance R was recorded every 0.02 s both during stretching and during release to obtain a continuous record of performance. The response and recovery times were measured by applying tension to the sample until it reached the desired strain value, maintaining this strain for 1 s, and then releasing the applied force and maintaining this relaxed state for 10 s. During this cycle, the strain−response and strain−recovery speeds were equivalent to the pulling speed (stretching speed) of 30 mm s^{-1}. During the test, the electrical resistance of the specimen was measured every 0.02 s.

3. RESULTS AND DISCUSSION

3.1. Single-Layer Strain Sensors. The neat PVNR films (i.e., 1-PVNR0.5mm, and 2-PVNR1.0mm) were used as the control samples to confirm the nonconductive properties and mechanical properties of AB-free rubber. Optical microscopic images revealed light gray surfaces for the control samples (Figure 2a,b), in contrast to the black surfaces of the 1-layer sensors 3-CNR0.5mm and 4-CNR1.0mm (Figure 2c,d). In addition, the surfaces of the sensors were not as smooth as those of the control samples (Figure 2a−d). This difference in smoothness was attributed to the presence of carboxymethyl cellulose (CMC) in the sensory films. The CMC increased the viscosity of the mixture, promoting air entrapment during mixing, and the air bubbles rose to the surface during drying to create a rougher surface for the two sensor films (i.e., 3-CNR0.5mm and 4-CNR1.0mm).

For the same sample composition, the film thickness (Table 3) increased with increased height of the applicator gap (Figure 1), resulting in an increased total volume of the film and an increased total quantity of AB recovered from 1-layered CNR films (3-CNR0.5mm and 4-CNR1.0mm; Table 3). The AB content of the films was measured as explained in Supporting Information (Section S1 and Figure S1). For

https://doi.org/10.1021/acsapm.5c02305
ACS Appl. Polym. Mater. 2025, 7, 12468−12479

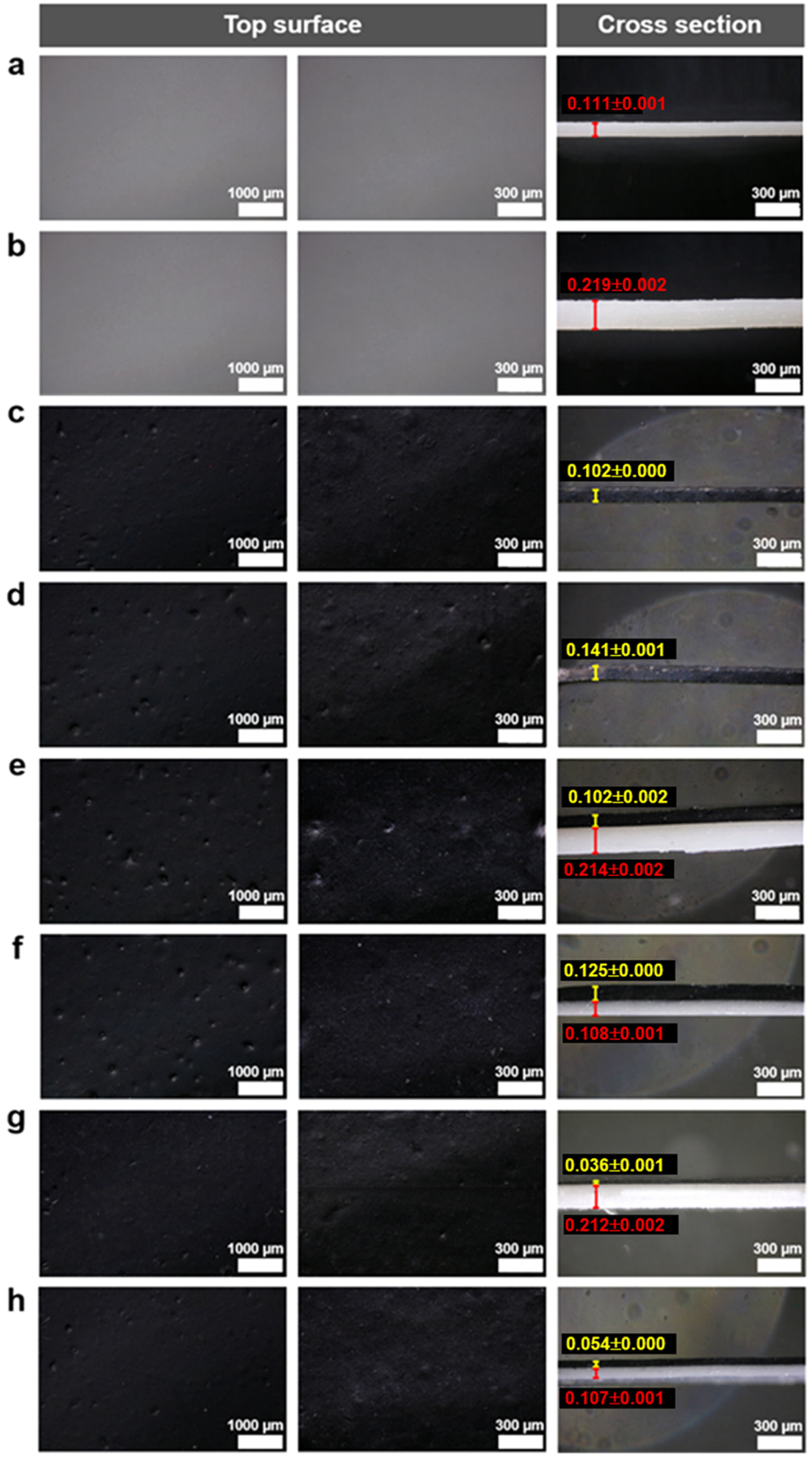

Figure 2. Optical microscopic images of the top surface (left and middle columns show the surface at different magnifications as on the scale bars) and the cross-section (right column) of neat PVNR films (1-PVNR0.5mm (a), and 2-PVNR1.0mm (b)) and the strain sensors: (c) 3-CNR0.5mm; (d) 4-CNR1.0mm; (e) 5-PVNR1.0mmCNR1.0mm; (f) 6-PVNR0.5mmCNR1.0mm; (g) 7-PVNR1.0mmCNR0.5mm; and (h) 8-PVNR0.5mmCNR0.5mm. The yellow and red bars indicate thicknesses (μm) of the CNR and PVNR layers, respectively.

https://doi.org/10.1021/acsapm.5c02305
ACS Appl. Polym. Mater. 2025, 7, 12468−12479

Table 3. Layer Thicknesses and the Acetylene Black (AB) Content of the Fabricated Strain Sensors

sample[a]	film applicator gap height (mm)		dry film thickness (mm)			AB (mg)	AB (% w w^{-1})
	PVNR layer	CNR layer	PVNR layer	CNR layer	total thickness		
1-PVNR0.5mm	0.5	-	0.111 ± 0.001	-	0.111 ± 0.001	0.0	0.00
2-PVNR1.0mm	1.0	-	0.219 ± 0.002	-	0.219 ± 0.002	0.0	0.00
3-CNR0.5mm	-	0.5	-	0.102 ± 0.000	0.102 ± 0.000	6.1	5.82
4-CNR1.0mm	-	1.0	-	0.141 ± 0.001	0.141 ± 0.001	11.7	5.88
5-PVNR1.0mmCNR1.0 mm	1.0	1.0	0.214 ± 0.002	0.102 ± 0.001	0.316 ± 0.002	11.0	2.69
6-PVNR0.5mmCNR1.0mm	0.5	1.0	0.108 ± 0.001	0.125 ± 0.000	0.234 ± 0.001	11.4	3.17
7-PVNR1.0mmCNR0.5mm	1.0	0.5	0.212 ± 0.002	0.036 ± 0.001	0.248 ± 0.002	4.9	1.38
8-PVNR0.5mmCNR0.5mm	0.5	0.5	0.107 ± 0.001	0.054 ± 0.000	0.161 ± 0.001	5.5	2.66

[a]In the *x*-*y*Az*B* format of the sample nomenclature, *x* denoted the sample number, the *y* specified the layer type (either PVNR or CNR), and *z* indicated the CNR layer. The layers *y* and *z* were formed using applicators with the specified gap heights (mm) of A and B, respectively.

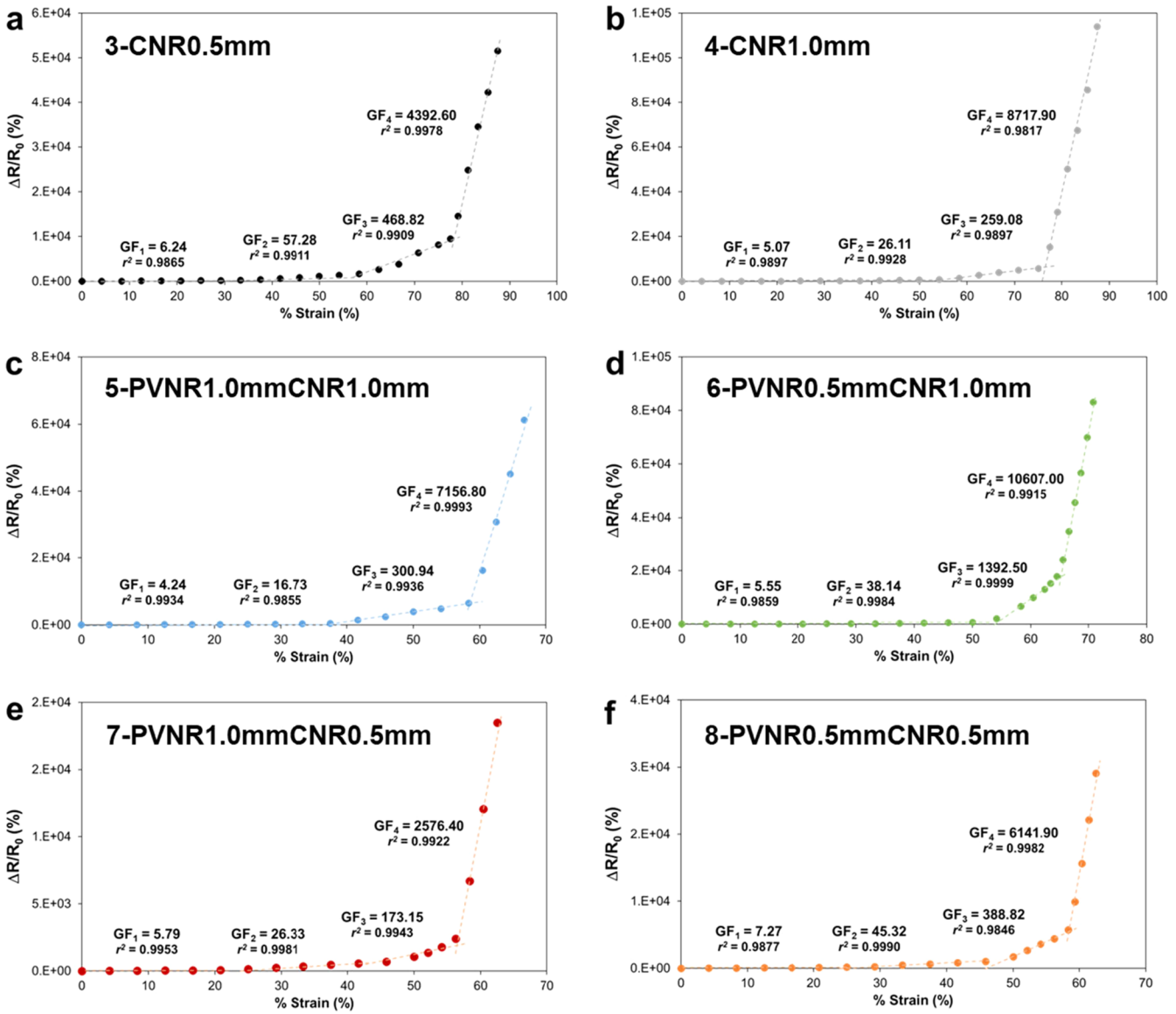

Figure 3. Change in relative resistance versus applied strain for the sensors: (a) 3-CNR0.5mm; (b) 4-CNR1.0mm; (c) 5-PVNR1.0mmCNR1.0mm; (d) 6-PVNR0.5mmCNR1.0mm; (e) 7-PVNR1.0mmCNR0.5mm; and (f) 8-PVNR0.5mmCNR0.5mm. Beyond the maximum strain values shown in the plots, the resistance values exceeded the instrument's upper detection limit of 10^8 Ω and could not be recorded. The straight lines with the linear correlation coefficients (r^2) values indicate the linearity of the sensor response over specific ranges of the applied strain. The *GF* values for the different strain ranges are shown.

https://doi.org/10.1021/acsapm.5c02305
ACS Appl. Polym. Mater. 2025, 7, 12468−12479

films prepared using an applicator of a given gap height, the 1-layer dry sensory film was always a little thinner than the dry film made using the neat PVNR (Table 3). This was because of the inclusion of CMC in the CNR latex formulation. The water-absorbing properties of CMC and its mesh-like structure[26] in solution, swelled the aqueous medium to increase the volume of the latex. Consequently, the solids concentration in the CNR latex was less than the concentration in the PVNR latex used in making the neat PVNR films. The wet films of the same initial dimensions made using an applicator of a given gap height resulted in thinner dry films (less total solids) of the CNR latex compared to the dry films of the PVNR latex.

3.1.1. Properties of Fabricated Sensors. The relevant mechanical properties (tensile strength, elongation at break, the various moduli) of the sensors are summarized in Table S1 (see Supporting Information). The 1-layer sensors with relatively high mass percentages of AB (i.e., 3-CNR0.5mm, and 4-CNR1.0mm; Table S1) had reduced tensile strength and elongation at break compared to the neat PVNR films of equal thickness; however, this reduction was compensated by enhanced moduli at 100%, 300%, and 500% elongation. The improved moduli were attributed to the carbon filler reducing the mobility of the rubber molecules in the polymer matrix.[27]

With respect to electrical properties, the control samples (i.e., the neat PVNR films) that lacked AB had high values of electrical resistance (R_0 greater than the instrument's limit of 10^8 Ω). In contrast, the 1-layer sensors were more conductive with R_0 values of the order of 10^5 Ω. The electrical resistance of these sensors increased under applied strain because of disconnection of some of the conductive links among the overlapping AB nanoparticles reduced, a common characteristic of strain sensors.[18,28] The 1-layer sensors exhibited different values of the gauge factor (*GF*) depending on the ranges of strain (Figure 3a,b), reflecting changes in sensing mechanisms. At low applied strain values, only some of the carbon particles in AB aggregates were pulled apart a short distance allowing electron transfer with minimal tunneling effect, a quantum mechanical phenomenon that enables electrons to travel a small distance through a nonconductive polymer matrix separating the carbon aggregates.[2,29] The low applied strain condition resulted in lower *GF* values. At higher strains more AB aggregates were disconnected and pulled further apart, reducing the tunneling effect and significantly increasing the *GF*.[18,30]

The 1-layer sensor 4-CNR1.0mm had a thicker CNR layer and a higher AB content than the sensor 3-CNR0.5mm; it also had lower *GF* values than 3-CNR0.5mm at lower strains but higher *GF* values at higher strains. This behavior was attributed to the thicker CNR layer with its more conductive pathways requiring greater strain to disrupt.[31] Furthermore, the disruption of these numerous pathways led to a pronounced increase in electrical resistance and, therefore, higher *GF* values.[31] Both 1-layer sensors (i.e., 3-CNR0.5mm, and 4-CNR1.0mm) were characterized by strong linear correlations between $\Delta R/R_0$ and strain, with the r^2 values exceeding 0.98 across all strain ranges (Figure 3a,b). However, the dynamic performance of these sensors was poor: the sensor 3-CNR0.5mm failed after 300 cycles whereas the sensor 4-CNR1.0mm failed after 600 cycles (Figure S2a,b; see Supporting Information). These failures were due to the tearing of the films.

3.2. Two-Layer Strain Sensors. The 2-layer sensor consisted of two parallel tightly adhering rubber layers: a nonconductive layer (the PVNR layer) produced from the PVNR latex, and a conductive layer (the CNR layer) produced from the CNR latex. The layers were formed as previously explained (Section 2.3 and Figure 1). Cross-sectional images (Figure 2e–h, column 3) revealed a clear interface between the lower PVNR layer and the upper CNR layer. The layers adhered tightly with no evidence of trapped air bubbles at the interface. However, the tiny indentations were observed on the outer surface of the CNR layer (Figure 2e–h; columns 1 and 2) suggesting that air bubbles existed in this layer. These bubbles likely originated from the inclusion of CMC in the CNR latex: CMC increased the viscosity of the latex and the microbubbles of air incorporated in the latex during mixing could not completely leave the viscous matrix. While drying with heating, the viscosity reduced because of the heat while the matrix was still liquid, and the trapped air bubbles migrated upward and burst at the surface leaving a pockmarked surface. The gap heights of the film applicators and the resulting dried layers are noted in Table 3.

3.2.1. Properties of Fabricated Sensors. The mechanical properties of the 2-layer sensors are summarized in Table S1 (see Supporting Information). Compared with 1-layer sensors, the 2-layer sensors had greater tensile strength and elongation at break (Table S1, see Supporting Information). For given thickness of the PVNR layer, the moduli of the 2-layer sensors increased with increasing thickness of the CNR layer, reflecting the contribution of the filler-rich CNR layer to the overall mechanical performance. Furthermore, the 2-layer sensor 6-PVNR0.5mmCNR1.0mm (Table S1, see Supporting Information) made by coating the CNR layer onto a partly dried PVNR layer exhibited better mechanical properties than the equivalent sample that was made by separately casting and drying the two films and then bringing them into contact as a bilayer (i.e., the unadhered 2-layer sample PVNR0.5mmCNR1.0mm; Table S1) clamped in the grips of the mechanical test equipment. In the sample with the nonadhering layers, the individual layers failed at different rates, with the conductive layer failing seconds before the PVNR layer. In contrast, in the sensors in which the second layer was coated before the first layer dried fully, both layers broke simultaneously, as observed visually. These results were clear evidence for strong interfacial adhesion between the layers when the CNR layer was coated on a partly dried PVNR layer.

In terms of electrical properties, the 2-layer sensors had R_0 (i.e., resistance in the absence of applied strain) values comparable to those of the 1-layer sensors (~10^5 Ω). Like the 1-layer sensors, the *GF* values of the 2-layer sensors varied with strain (Figure 3c–f). For 2-layer sensors, the *GF* increased with the applied strain and with the thickness of the CNR layer (Figure 3c–f and Table 3). In contrast, the thickness of the PVNR layer did not significantly affect *GF* values of the 2-layer sensors (Figure 3c–f and Table 3). The sensors demonstrated excellent linearity (r^2 > 0.98) of electrical response for wide ranges of strain.

All sensors with the same total AB content demonstrated comparable sensitivity irrespective of the number of layers (Figure 3a–f). For example, the 4-CNR1.0mm (1-layer sensor), the 5-PVNR1.0mmCNR1.0mm (2-layer sensor), and 6-PVNR0.5mmCNR1.0mm (2-layer sensor) had similar total AB content (Table 3), and similar *GF* values. These *GF* values

https://doi.org/10.1021/acsapm.5c02305
ACS Appl. Polym. Mater. 2025, 7, 12468–12479

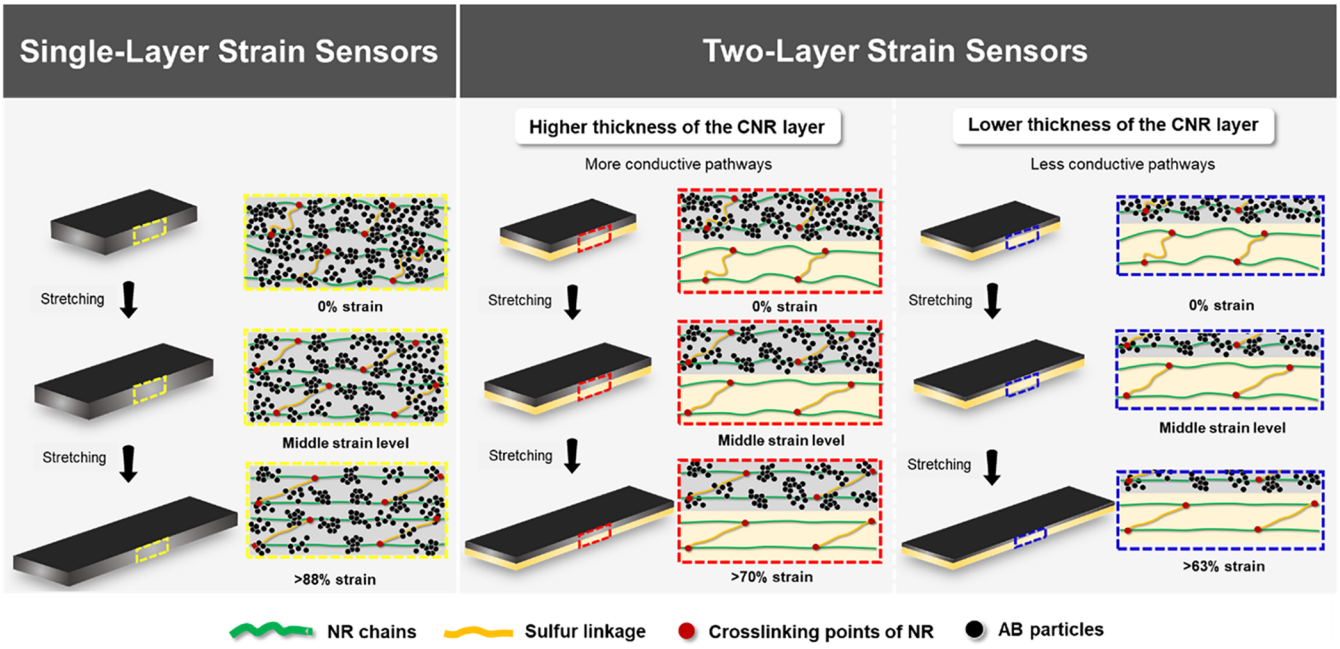

Figure 4. Schematic illustration of the sensing mechanism in single-layer and bilayer strain sensors.

were notably higher than those of the sensors with lower total AB content (i.e., the sensors 3-CNR0.5mm (1-layer sensor), 7-PVNR1.0mmCNR0.5mm (2-layer sensor), and 8-PVNR0.5mmCNR0.5mm (2-layer sensor)). A higher *GF* for the sensor with a higher AB loading was consistent with the literature.[31] Among all samples, the 2-layer sensor 6-PVNR0.5mmCNR1.0mm had the highest *GF* value (10,607; Figure 3d) and an outstanding durability, enduring 5,000 stretch−release cycles (see further details in Section 3.3).

Compared to single-layer sensors, the bilayer configurations demonstrated superior overall performance. The bilayer sensors exhibited greater tensile strength and elongation at break (Table S1) and withstood repeated stretching cycles within the tested strain range far beyond the failure points observed in single-layer sensors (Figure S2a,b). These results indicated that the bilayer design effectively preserved the intrinsic rubber elasticity of PVNR, enabling full recovery after deformation and substantially enhancing the sensor's durability.

A schematic representation of the sensing mechanism is shown in Figure 4. Although the single-layer and the bilayer sensors exhibited different dynamic durability, both demonstrated comparable *GF* values, indicating that their sensing mechanisms were fundamentally the same. In all strain sensors, regardless of the number of layers or the thickness of the CNR layer, the separation among AB aggregates increased with applied strain. At low strain levels, the aggregates were only slightly displaced, and electrons could move between the filler particles via the tunneling effect. As a result, the *GF* remained relatively low in this strain regime. However, as the strain increased, the AB aggregates were pulled farther apart, disrupting more of the conductive pathways and significantly reducing the tunneling effect. This led to a pronounced increase in electrical resistance and, consequently, a higher *GF* at larger strains. At a sufficiently high strain, the conductive network was fully disrupted, and the electrical resistance exceeded the measurement limit of the instrument.

Regarding the effect of the thickness of the CNR layer, increasing thickness effectively increased the total amount of conductive filler, thereby increasing the initial number of conductive pathways.[18,31] With more filler present, higher strain was required to fully separate the AB aggregates and suppress the tunneling effect. In other words, sensors with thicker CNR layers could withstand greater deformation before losing conductivity. In addition, at sufficiently high strain, the larger number of conductive pathways available for disruption in sensors with thicker CNR layers resulted in higher *GF* values compared to sensors with thinner CNR layers.

Notably, the *GF* value of the 2-layer sensor 6-PVNR0.5mmCNR1.0mm was high compared to the literature for a stretchable strain sensor operating within a 100% strain range.[11−13,32] Furthermore, the sensor 6-PVNR0.5mmCNR1.0mm had a high flexibility considering its low measured value of Young's modulus (0.06 MPa).[29,33,34] Overall, the 2-layer sensor 6-PVNR0.5mmCNR1.0mm was deemed optimal and all subsequent work focused on this configuration.

3.3. Static and Dynamic Characteristics of the Optimal Sensor 6-PVNR0.5mmCNR1.0mm.

3.3.1. Hysteresis Tests. Hysteresis, or the difference in $\Delta R/R_0$ during stretching and retraction in the strain range of 0−71% (Figure 5a), reflects the energy loss due to softening or deformation of material.[35] The degrees of hysteresis (*DH*) declined sharply after two cycles and then stabilized at ∼4.4% (Table 4), well below the 20% upper threshold for an ideal sensor for applications involving rapid contraction.[32] Hysteresis is influenced by the viscoelasticity of a polymer matrix and the strength of interfacial adhesion between the polymer matrix and the conductive particles.[1,36] The stable *DH* observed after two cycles suggested that the initial stretching broke the weak adhesive links between the polymer and the conductive particles, leaving the polymer's viscoelasticity as the primary factor influencing hysteresis. After the initial two stretch−release cycles, hysteresis was essentially absent in the optimal

https://doi.org/10.1021/acsapm.5c02305
ACS Appl. Polym. Mater. 2025, 7, 12468−12479

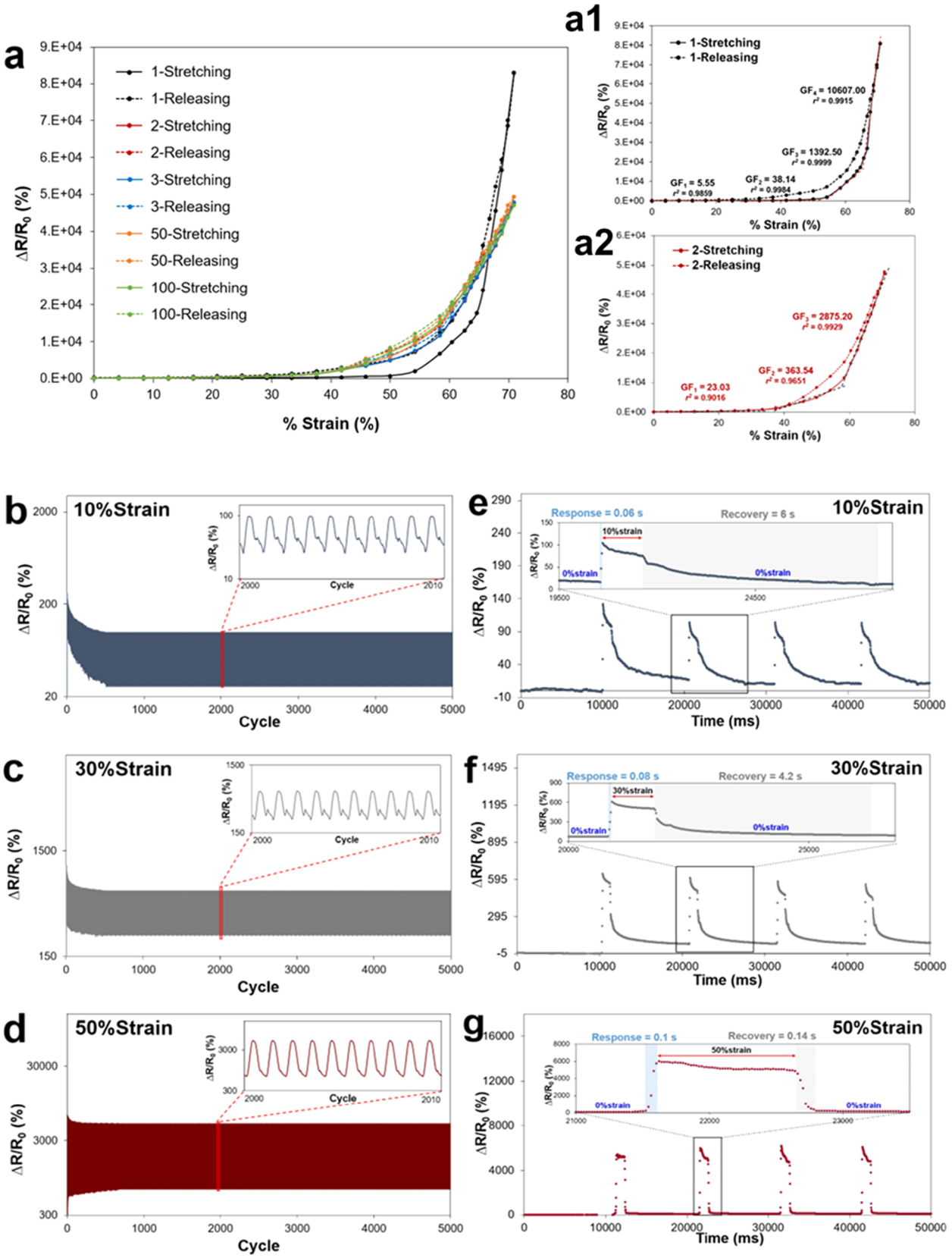

Figure 5. Static and dynamic characteristics of the 6-PVNR0.5mmCNR1.0mm sensor. (a) $\Delta R/R_0$ versus strain for 100 cycles (the insets a1 and a2 show the data for the first and the second stretch−release cycles). The *GF* values shown were obtained during stretching. The dynamic durability tests over 5000 cycles for strains of: (b) 10%; (c) 30%; and (d) 50%. Response and recovery times of the sensor under transient input at strains of: (e) 10%; (f) 30%; and (g) 50%.

https://doi.org/10.1021/acsapm.5c02305
ACS Appl. Polym. Mater. 2025, 7, 12468−12479

Table 4. Electrical Properties and Sensory Performance Characteristics of the Sensor 6-PVNR0.5mmCNR1.0mm in the Strain Range of 0−71%

cycle number	*DH* (%)	R_0 (Ω)	*GF* (% strain range)	r^2 (stretch)[a]
1	33.5	1.40×10^5	5.55 (0−33%)	0.9859
			38.14 (33−50%)	0.9984
			1392.50 (50−64%)	0.9999
			10607.00 (64−71%)	0.9915
2	8.3	2.41×10^5	23.03 (0−33%)	0.9016
			363.54 (33−54%)	0.9651
			2875.2 (54−71%)	0.9929
3	4.4	2.40×10^5	23.59 (0−33%)	0.9471
			365.06 (33−54%)	0.9651
			2887.2 (54−71%)	0.9929
50	4.4	2.31×10^5	23.61 (0−33%)	0.9429
			397.02 (33−54%)	0.9832
			2795.6 (54−71%)	0.9931
100	4.4	2.41×10^5	24.00 (0−33%)	0.9003
			422.95 (33−54%)	0.9889
			2795.40 (54−71%)	0.9972

[a] r^2 is the linear correlation coefficient in the specified range of the applied strain.

sensor configuration because the rubber used had been vulcanized to prevent permanent creep.

As noted earlier, the initial stretch cycle caused a partial disruption of the conductive network. This initially increased and then stabilized the R_0 value (Table 4 and Figure 5a). Similarly, the *GF* value initially decreased and then stabilized (Table 4 and Figure 5a). The R_0 value of the optimal sensor increased from 1.40×10^5 Ω (Cycle 1) to 2.41×10^5 Ω (Cycles 2, ···, 100), whereas the peak *GF* value in Cycle 1 decreased from ∼10,600 to ∼2800 (Cycles 2−100). Further repeated cycles (Cycle ≥ 2) did not affect the sensor linearity, ensuring consistent performance (Table 4). Thus, prior to use in routine measurements, the sensor required at least two stretch cycles to stably realign the conductive material[37] in the polymer matrix.

3.3.2 Dynamic Durability Tests. These tests characterize the useful life of a sensor by subjecting it repeated loading−unloading cycles in the 10−50% strain range (Figure 5b−d). After the initial stabilization cycles, the sensor attained a stable resistive response pattern (i.e., $\Delta R/R_0$ values) (Figure 5b−d) comparable to patterns reported for other strain sensors.[28,38] Thus, after the initial cycles, a stable conductive network emerged with the same conductive pathways connecting and disconnecting during repeated loading−unloading cycles.[28,37] Larger strains increased $\Delta R/R_0$ values (Figure 5b−d) as the conductive network was disrupted more severely, increasing the interspacing among the carbon aggregates. In addition, the hysteretic behavior, evidenced by dual peaks within individual cycles, was most pronounced at 10% and 30% strain and disappeared at 50% strain (Figure 5b−d). The larger peak occurred at maximum extension, while the smaller shoulder peak appeared during retraction. This was attributed to weak filler−polymer adhesion resulting in slippage of the AB aggregates during retraction, with a consequent increase in resistance.[1,11,28] At higher strains, the retractive force in the cross-linked rubber matrix, driven by entropy loss,[39] counteracted slippage, reducing hysteresis. However, at strains ≥60%, the sensor stability declined due to severe damage to the conductive network (Figure S3; see Supporting Information).

Response time and the recovery time of the sensor stabilized after the first loading−unloading cycle in the 10−50% strain range (Table 5) because of the above-discussed changes in the conductive network (see Section 3.3.1). After the first cycle, the response time correlated linearly with strain ($r^2 \approx 1$). The recovery times were larger than the response times because of the friction between the polymer matrix and the filler,[1] but decreased linearly with increasing strain. This was attributed to the entropy loss within the rubber matrix creating a stronger retractive force to overcome friction and enabling a rapid return to the original state.[39] The recovery times at 50% strain (0.14−0.16 s) were consistent with data reported for other natural rubber-based sensors (e.g., 0.1−0.135 s).[21] Resistive relaxation occurred, as evidenced by a decrease in $\Delta R/R_0$ under constant tensile strain (Figure 5e−g). This behavior is typical of viscoelastic polymers.[11,37]

Table 5. Response and Recovery Times of the Sensor 6-PVNR0.5mmCNR1.0mm for Various Applied Strains and Use Cycles

strain (%)	cycle number	response time (s)	recovery time (s)
10	1	0.06	6.50
10	2	0.06	6.00
10	40 (last cycle)	0.06	6.00
30	1	0.10	4.60
30	2	0.08	4.20
30	40 (last cycle)	0.08	4.20
50	1	0.12	0.16
50	2	0.10	0.14
50	40 (last cycle)	0.10	0.14

Based on the SEM images (Figure 6a−c), the surface of the sensor 6-PVNR0.5mmCNR1.0mm showed no change, or damage, after 5000 loading−unloading cycles at 50% strain (Figure 6c), compared to both the initial state (Figure 6a) and after one use cycle (Figure 6b). Similarly, the cross-sectional image after 5000 cycles (Figure 6f) revealed no signs of cracking or delamination between the PVNR and CNR layers and was comparable to the initial (Figure 6d) and post-first-cycle (Figure 6e) images. This confirmed the presence of strong interfacial adhesion, likely because the CNR layer was applied before complete drying of the PVNR layer, resulting in polymer chain interdiffusion and mechanical interlocking. Thus, the 2-layer optimal sensor was robust.

A transmission electron microscopy (TEM) image of the film made from S-PVNR latex without the conductive filler is shown in Figure 7a. Spherical rubber particles (0.5 to 1 μm in size) and the dispersed ZnO particles are visible in the image (Figure 7a). The image in Figure 7a is comparable to other published images of S-PVNR latex.[14] The TEM image of the sensor 6-PVNR0.5mmCNR1.0mm (Figure 7b) showed dispersed AB aggregates in addition to the clusters of spherical rubber particles and ZnO particles. As Figure 7b was a 2D image it could not show the conductive network but fine AB particles could be seen in the interspaces of the NR particles.

Compared to prior work on the preparation of sulfur-prevulcanized natural rubber latex,[14] the present study used a different method of incorporating the conductive filler. The earlier work used an embedding technique in combination with a high loading (12 phr) of the filler to produce a sensor with a

https://doi.org/10.1021/acsapm.5c02305
ACS Appl. Polym. Mater. 2025, 7, 12468−12479

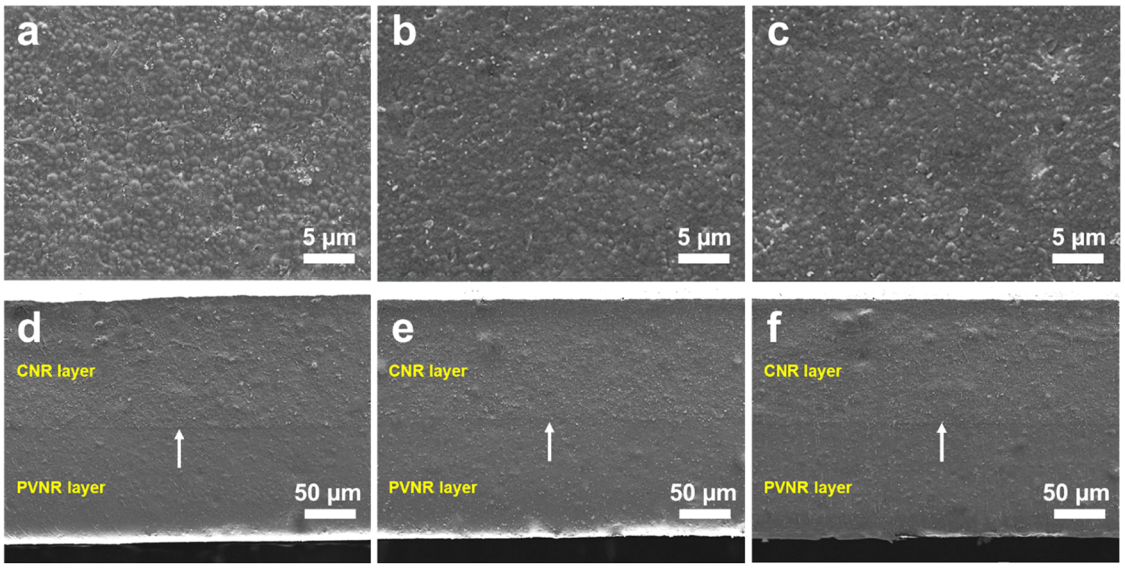

Figure 6. SEM images of the top surface (top row) and the cross-section (bottom row) of the sensor 6-PVNR0.5mmCNR1.0mm: initial state (a, d); after 1 cycle (b, e); and after 5000 cycles (c, f). The applied strain was 50% at a strain rate of 30 mm s^{-1}. The white arrows (d, e, f) identify the interface between the layers.

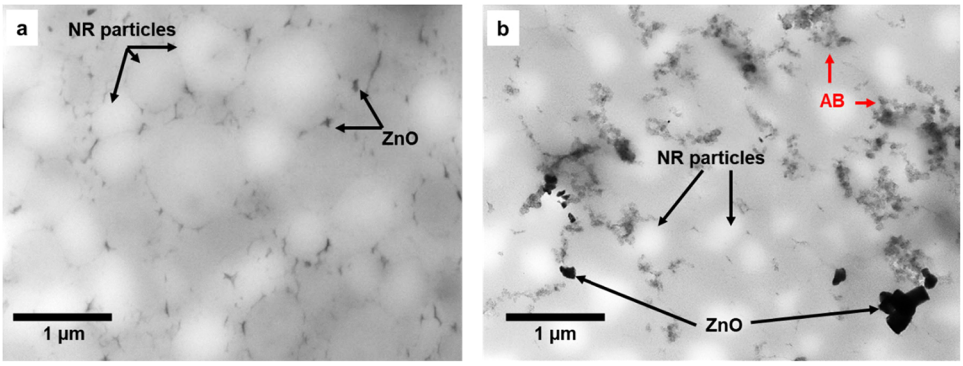

Figure 7. TEM images of (a) 1-PVNR0.5mm film; and (b) the prepared sensor 6-PVNR0.5mmCNR1.0mm. Globules of natural rubber (NR), zinc oxide (ZnO) particles and acetylene black (AB) particles are shown.

gauge factor (*GF*) of only 9.71 (0−140% strain) and a tensile strength of 12 MPa.[14] In contrast, the optimized sensor 6-PVNR0.5mmCNR1.0mm in the present work achieved much higher performance values (Table S1 and Table 4), despite using a filler loading of only 5 phr. In addition, the *GF* performance of the optimized sensor in this work exceeded that reported in several previous studies.[9,21,22]

Certain strain sensors fabricated using a bilayer configuration were reported to have *GF* values ranging from around 10 to nearly 1265 in the strain range of 0−80%.[9] These sensors were successfully applied to monitor various human motions, including pulse, swallowing, tiptoeing, and joint movements.[9] The strain associated with these types of motions typically falls within the 3% to 100% range.[18,40] In addition, strain sensors with hysteresis (*DH*) values below 20% have been shown to be reliable over thousands of dynamic stretching cycles.[11,13,18,32,38] In comparison with these earlier sensors, the optimized sensor 6-PVNR0.5mmCNR1.0mm of the present study exhibited excellent sensitivity, comparable hysteresis behavior, and outstanding dynamic durability. These attributes suggest it has strong potential for future applications in human motion monitoring and wearable electronics.

4. CONCLUSIONS

A highly stretchable strain sensor based on natural rubber films was developed. The sensor had a 2-layer structure consisting of a nonconductive prevulcanized natural rubber (PVNR) layer and an adhering carbon-composited conductive natural rubber (CNR) layer both having precise thicknesses. Both layers were prepared using a sulfur-prevulcanized NR latex to enhance the mechanical strength and elasticity of the sensor and reduce polymer creep. A reduced creep reduced hysteresis during repeated stretch−release cycles. In terms of the mechanical properties, sensitivity, reproducibility, stability, and durability, the optimized 2-layer sensor outperformed an identically thick 1-layer sensor made of CNR. While the 1-layer sensor failed after 300−600 cycles during durability tests, the 2-layer sensor had excellent long-term stability (>5000 cycles at 10−50% strain). The 2-layer sensor had a high gauge factor (*GF*) value of 10607 under 64−71% strain during the first use cycle, stabilizing at ∼2800 from the second cycle onward (54−71% strain). This confirmed the need for pre-stretching before use. The 2-layer sensor had a short response time (0.10 s) and recovery time (0.14 s at 50% strain), and satisfactory hysteresis characteristics. The high sensitivity of the 2-layer sensor was a consequence of an optimally thick conductive rubber layer,

https://doi.org/10.1021/acsapm.5c02305
ACS Appl. Polym. Mater. 2025, 7, 12468−12479

while the PVNR layer provided the required durability. The SEM images revealed strong adhesion between the PVNR layer and the CNR layer even after 5000 stretching cycles at 50% strain. Given its high sensitivity, mechanical robustness, low cost, and flexibility, the bilayer NR-based strain sensor has a strong potential for wearable applications, particularly for human motion detection. Future work may explore the influence of CMC as a dispersant on sensory performance and the sensor's stability in biologically relevant environments (e.g., sweat) for wearable applications.

■ ASSOCIATED CONTENT

Supporting Information

The Supporting Information is available free of charge at https://pubs.acs.org/doi/10.1021/acsapm.5c02305.

AB determination, mechanical properties for all sensors, and dynamic durability tests of 3-CNR0.5mm and 4-CNR1.0mm (PDF)

■ AUTHOR INFORMATION

Corresponding Authors

Panithi Wiroonpochit − *National Metal and Materials Technology Center, National Science and Technology Development Agency (NSTDA), Pathum Thani 12120, Thailand;* orcid.org/0000-0001-6669-0727; Email: panithiw@mtec.or.th

Sasitorn Srisawadi − *National Metal and Materials Technology Center, National Science and Technology Development Agency (NSTDA), Pathum Thani 12120, Thailand*; Email: sasitors@mtec.or.th

Nanthiya Hansupalak − *Department of Chemical Engineering, Faculty of Engineering, Kasetsart University, Bangkok 10900, Thailand; Specialized Center of Rubber and Polymer Materials for Agriculture and Industry, Faculty of Science, Kasetsart University, Bangkok 10900, Thailand;* orcid.org/0000-0002-9917-403X; Email: fengnyh@ku.ac.th

Authors

Sutthinee Keawmaungkom − *Department of Chemical Engineering, Faculty of Engineering, Kasetsart University, Bangkok 10900, Thailand; National Metal and Materials Technology Center, National Science and Technology Development Agency (NSTDA), Pathum Thani 12120, Thailand*

Siwaporn Srimongkol − *National Metal and Materials Technology Center, National Science and Technology Development Agency (NSTDA), Pathum Thani 12120, Thailand*

Jirasak Wong-Ekkabut − *Department of Physics, Faculty of Science and Computational Biomodelling Laboratory for Agricultural Science and Technology (CBLAST), Faculty of Science, Kasetsart University, Bangkok 10900, Thailand*

Saree Phongphanphanee − *Computational Biomodelling Laboratory for Agricultural Science and Technology (CBLAST), Faculty of Science and Department of Material Science, Faculty of Science, Kasetsart University, Bangkok 10900, Thailand*

Sarun Phibanchon − *Department of Innovation and Educational Technology, Faculty of Education, Burapha University, Chonburi 20131, Thailand*

Yusuf Chisti − *Department of Chemical Engineering, Faculty of Engineering, Kasetsart University, Bangkok 10900, Thailand; Institute of Tropical Aquaculture and Fisheries, Universiti Malaysia Terengganu, 21030 Kuala Nerus, Terengganu, Malaysia*

Complete contact information is available at: https://pubs.acs.org/10.1021/acsapm.5c02305

Author Contributions

S.K.: Conceptualization, Methodology, Investigation, Writing−Original Draft, Writing−Review Editing. P.W.: Conceptualization, Methodology, Investigation, Resources, Writing−Review Editing, Visualization, Funding acquisition. S.S.: Conceptualization, Methodology, Investigation, Resources, Writing−Review Editing, Visualization, Funding acquisition. Si.S.: Methodology, Investigation. J.W.-E.: Visualization, Funding acquisition. S.Pho.: Visualization, Funding acquisition. S.Phi.: Visualization, Funding acquisition. Y.C.: Writing−Review Editing, Visualization. N.H.: Conceptualization, Methodology, Investigation, Resources, Writing−Original Draft, Writing−Review Editing, Visualization, Supervision, Project administration, Funding acquisition.

Notes

The authors declare no competing financial interest.

■ ACKNOWLEDGMENTS

Financial support from the following sources is gratefully acknowledged: the Kasetsart University Research and Development Institute (KURDI) through Fundamental Fund (grant no. FF(KU)33.67); the NSRF via the Program Management Unit for Human Resources Institutional Development, Research and Innovation (grant number B42G670041); and IRPC Public Co., Ltd., Thailand, for gifting the conductive filler.

■ REFERENCES

(1) Dogu, M.; Alanalp, M. B.; Durmus, A. Polymer Composites for Strain Sensors. In *Polymeric Nanocomposite Materials for Sensor Applications*; Parameswaranpillai, J.; Ganguly, S., Eds.; Elsevier, 2022; pp 381−404 DOI: 10.1016/B978-0-323-98830-8.00002-3.

(2) Souri, H.; Banerjee, H.; Jusufi, A.; Radacsi, N.; Stokes, A.; Park, I.; Sitti, M.; Amjadi, M. Wearable and Stretchable Strain Sensors: Materials, Sensing Mechanisms, and Applications. *Adv. Intell. Syst.* **2020**, *2*, No. 2000039.

(3) Xiang, D.; Zhang, X.; Liu, Z.; Liu, L.; Wang, P.; Zhao, C.; Li, H.; Cheng, J.; Wang, B.; Wu, Y. Preparation and Performance of Biaxially Stretched CNT-SBS/POE Flexible Strain Sensor with a Double Percolation Structure. *Sens. Actuators, A* **2024**, *371*, No. 115340.

(4) Wang, J.; Lu, C.; Zhang, K. Textile-Based Strain Sensor for Human Motion Detection. *Energy Environ. Mater.* **2020**, *3*, 80−100.

(5) Yang, P.-a.; Liu, Z.; Zou, L.; Li, R.; Zhou, Z.; Deng, W.; Shou, M.; Wang, X.-Y.; Luo, J. Optimal Design and Fabrication of Stable Ordered Porous Conductive Structure for Flexible Strain Sensors With High Sensitivity and Linearity. *Diamond Relat. Mater.* **2023**, *136*, No. 109990.

(6) Ren, M.; Li, J.; Zhao, Y.; Zhai, W.; Zhou, K.; Yu, Y.; Wang, S.; Dai, K.; Liu, C.; Shen, C. Highly Strain-Sensitive and Stretchable Multilayer Conductive Composite Based on Aligned Thermoplastic Polyurethane Fibrous Mat for Human Motion Monitoring. *Compos. Commun.* **2024**, *46*, No. 101840.

(7) Xiang, D.; Li, J.; Li, Z.; Zhang, X.; Zhao, C.; Li, H.; Lai, J.; Wang, B.; Wang, P.; Li, D.; Wu, Y. Bilayer-Structured Carbon Nanotube/Ethylene−Vinyl Acetate Flexible Strain Sensors with Enhanced Sensing Performance Prepared by Biaxial Stretching. *Sens. Actuators, A* **2024**, *366*, No. 114992.

(8) Cai, Y.; Chen, D.; Cheng, L.; Guo, S.; Hu, Z.; Wang, Y.; Yu, H.; Zhou, Y. Preparation and Sensing Properties of Multiscale Conductive Filler Hybrid CNTs@Ag-MXene-TPU/TPU Double-Layer Strain Sensing Materials. *Composites, Part A* **2024**, *186*, No. 108430.
(9) Cui, X.; Miao, C.; Lu, S.; Liu, X.; Yang, Y.; Sun, J. Strain sensors made of MXene, CNTs, and TPU/PSF asymmetric structure films with large tensile recovery and applied in human health monitoring. *ACS Appl. Mater. Interfaces* **2023**, *15*, 59655−59670.
(10) Lin, L.; Wang, L.; Li, B.; Luo, J.; Huang, X.; Gao, Q.; Xue, H.; Gao, J. Dual Conductive Network Enabled Superhydrophobic and High Performance Strain Sensors with Outstanding Electro-Thermal Performance and Extremely High Gauge Factors. *Chem. Eng. J.* **2020**, *385*, No. 123391.
(11) Lin, H.; Zhang, C.; Liao, N.; Zhang, M. Microcracked Strain Sensor Based on Carbon Nanotubes/Copper Composite Film with High Performance and Waterproof Property for Underwater Motion Detection. *Composites, Part B* **2023**, *254*, No. 110574.
(12) Wan, B.; Yang, Y.; Yuan, Y.; Guo, R.; Yu, X. Functionalised Conductive Elastomers for Strain Monitoring of Seismic Isolation Bearings: Experiments and Molecular Simulations. *Eng. Sci.* **2025**, *34*, No. 1479.
(13) Kouediatouka, A. N.; Liu, Q.; Mawignon, F. J.; Wang, W.; Wang, J.; Ruan, C.; Yeo, K. F. H.; Dong, G. Sensing Characterization of an Amorphous PDMS/Ecoflex Blend Composites with an Improved Interfacial Bonding and Rubbing Performance. *Appl. Surf. Sci.* **2023**, *635*, No. 157675.
(14) Srimongkol, S.; Wiroonpochit, P.; Utra, K.; Sethayospongsa, R.; Muthitamongkol, P.; Methachan, B.; Butsri, N.; Srisawadi, S. Carbon-Based Conductive Rubber Composite for 3D Printed Flexible Strain Sensors. *Polym. Adv. Technol.* **2023**, *34*, 287−298.
(15) Akhtar, I.; Chang, S.-H. Highly Aligned Carbon Nanotubes and their Sensor Applications. *Nanoscale* **2020**, *12*, 21447−21458.
(16) Xie, X.; Huang, H.; Zhu, J.; Yu, J.; Wang, Y.; Hu, Z. A Spirally Layered Carbon Nanotube-Graphene/Polyurethane Composite Yarn for Highly Sensitive and Stretchable Strain Sensor. *Composites, Part A* **2020**, *135*, No. 105932.
(17) Yu, R.; Zhu, C.; Wan, J.; Li, Y.; Hong, X. Review of Graphene-Based Textile Strain Sensors, with Emphasis on Structure Activity Relationship. *Polymers* **2021**, *13*, No. 151.
(18) Huang, J.; Li, Z.; Kang, T.; Wei, W.; Liu, F.; Xu, X.; Liu, Z. Fabrication of Styrene−Butadienestyrene (SBS) Matrix-Based Flexible Strain Sensors with Brittle Cellulose Nanocrystal (CNC)/Carbon Black (CB) Segregated Networks. *Compos. Struct.* **2023**, *320*, No. 117231.
(19) Monastyreckis, G.; Stepura, A.; Soyka, Y.; Maltanava, H.; Poznyak, S. K.; Omastová, M.; Aniskevich, A.; Zeleniakiene, D. Strain Sensing Coatings for Large Composite Structures Based on 2D Mxene Nanoparticles. *Sensors* **2021**, *21*, No. 2378.
(20) Liu, X.; Wu, Z.; Alomar, T. S.; AlMasoud, N.; Liu, X.; Han, X.; Guo, N.; Weng, L.; Gao, J.; Algadi, H.; Koibasova, L.; Ydyrys, A.; Ren, J.; Guo, Z. Poly (Vinyl Alcohol)/Carboxylated Cellulose Nanofibers Composite Hydrogel Flexible Strain Sensors. *Int. J. Biol. Macromol.* **2025**, *309*, No. 142902.
(21) Zhang, Z.; Zhou, M.; Yu, P.; Wu, Z. Recent Advances and Future Prospects of Flexible Sensors Based on Natural Rubber. *Int. J. Biol. Macromol.* **2025**, *320*, No. 145821.
(22) Georgopoulou, A.; Srisawadi, S.; Wiroonpochit, P.; Clemens, F. Soft Wearable Piezoresistive Sensors Based on Natural Rubber Fabricated with a Customized Vat-Based Additive Manufacturing Process. *Polymers* **2023**, *15*, No. 2410.
(23) Polimaxx. AB50P Acetylene Black (AB), L. IRPC Public Co., Thailand, 2011 https://polimaxx.irpc.co.th/wp-content/uploads/2022/09/ab_ab50p_datasheet.pdf.
(24) Deng, Z.; Li, H.; Tian, Q.; Zhou, Y.; Yang, X.; Yu, Y.; Jiang, B.; Xu, Y.; Zhou, T. Electrochemical Detection of Methotrexate in Serum Sample Based on the Modified Acetylene Black Sensor. *Microchem. J.* **2020**, *157*, No. 105058.
(25) Wang, R.; Yi, H. Mechanical-Induced Functionalization of Graphene with Sodium Carboxymethyl Cellulose Toward Enhancing Anticorrosion Performance of Waterborne Epoxy Coatings. *J. Coat. Technol. Res.* **2023**, *20*, 2069−2080.
(26) Blackley, D. C. Natural Latices. In *Polymer Latices: Science and Technology, Vol. 2: Types of Latices*; Blackley, D. C., Ed.; Springer, 1997; pp 1−136 DOI: 10.1007/978-94-011-5866-4_1.
(27) Wiroonpochit, P.; Keawmaungkom, S.; Chisti, Y.; Hansupalak, N. A Novel Preparation of Natural Rubber Films with a Conducting Nanocarbon Network for Antistatic Applications. *Mater. Today Commun.* **2023**, *34*, No. 105349.
(28) Duan, L.; Spoerk, M.; Wieme, T.; Cornillie, P.; Xia, H.; Zhang, J.; Cardon, L.; D'Hooge, D. R. Designing Formulation Variables of Extrusion-Based Manufacturing of Carbon Black Conductive Polymer Composites for Piezoresistive Sensing. *Compos. Sci. Technol.* **2019**, *171*, 78−85.
(29) Lu, Y.; Biswas, M. C.; Guo, Z.; Jeon, J. W.; Wujcik, E. K. Recent Developments in Bio-Monitoring via Advanced Polymer Nanocomposite-Based Wearable Strain Sensors. *Biosens. Bioelectron.* **2019**, *123*, 167−177.
(30) Fan, M.; Wu, L.; Hu, Y.; Qu, M.; Yang, S.; Tang, P.; Pan, L.; Wang, H.; Bin, Y. A Highly Stretchable Natural Rubber/Buckypaper/Natural Rubber (NR/N-BP/NR) Sandwich Strain Sensor with Ultrahigh Sensitivity. *Adv. Compos. Hybrid Mater.* **2021**, *4*, 1039−1047.
(31) Bharadwaj, S.; Gupta, T. K.; Chauhan, G. S.; Sehrawat, M.; Kumar, A.; Dhakate, S. R.; Singh, B. P. Long Length MWCNT/TPU Composite Materials for Stretchable and Wearable Strain Sensors. *Sens. Actuators, A* **2023**, *357*, No. 114364.
(32) Khalid, M. A. U.; Chang, S. H. Flexible Strain Sensors for Wearable Applications Fabricated using Novel Functional Nanocomposites: A Review. *Compos. Struct.* **2022**, *284*, No. 115214.
(33) Amjadi, M.; Pichitpajongkit, A.; Lee, S.; Ryu, S.; Park, I. Highly Stretchable and Sensitive Strain Sensor Based on Silver Nanowire−Elastomer Nanocomposite. *ACS Nano* **2014**, *8*, 5154−5163.
(34) Yang, C.; Dong, J.; Fang, Y.; Ma, L.; Zhao, X.; Zhang, Q. Preparation of Novel Low-κ Polyimide Fibers with Simultaneously Excellent Mechanical Properties, UV-Resistance and Surface Activity using Chemically Bonded Hyperbranched Polysiloxane. *J. Mater. Chem. C* **2018**, *6*, 1229−1238.
(35) Liu, C.; Sun, Y.; Liu, P.; Ma, F.; Wu, S.; Li, J.; Li, S.; Hu, R.; Wang, Z.; Wang, Y.; Liu, G.; Xing, K.; Tian, H.; Huang, H.; Guo, X.; Ge, C.; Yang, X.; Huang, Y. Fabrication and Characterization of Highly Sensitive Flexible Strain Sensor Based on Biodegradable Gelatin Nanocomposites and Double Strain Layered Structures with Crack for Gesture Recognition. *Int. J. Biol. Macromol.* **2023**, *231*, No. 123568.
(36) Lin, L.; Park, S.; Kim, Y.; Bae, M.; Lee, J.; Zhang, W.; Gao, J.; Paek, S. H.; Piao, Y. Wearable and Stretchable Conductive Polymer Composites for Strain Sensors: How to Design a Superior One? *Nano Mater. Sci.* **2023**, *5*, 392−403.
(37) Natarajan, T. S.; Eshwaran, S. B.; Stöckelhuber, K. W.; Wießner, S.; Pötschke, P.; Heinrich, G.; Das, A. Strong Strain Sensing Performance of Natural Rubber Nanocomposites. *ACS Appl. Mater. Interfaces* **2017**, *9*, 4860−4872.
(38) Xia, P.; Liu, P.; Wu, S.; Zhang, Q.; Wang, P.; Hu, R.; Xing, K.; Liu, C.; Song, A.; Yang, X.; Huang, Y. Highly Stretchable and Sensitive Flexible Resistive Strain Sensor Based on Waterborne Polyurethane Polymer for Wearable Electronics. *Compos. Sci. Technol.* **2022**, *221*, No. 109355.
(39) Fried, J. R. *Polymer Science and Technology*, 3rd ed.; Prentice Hall, 2014.
(40) Zeng, W.; Shu, L.; Li, Q.; Chen, S.; Wang, F.; Tao, X. M. Fiber Based Wearable Electronics: A Review of Materials, Fabrication, Devices, and Applications. *Adv. Mater.* **2014**, *26*, 5310−5336.